The associative nature of adenylyl transfer catalyzed by T4 DNA ligase

Cherepanov, A.V.; Doroshenko, E.V.; Matysik, J.; Vries, S. de; Groot H.J.M. de

Note: To cite this publication please use the final published version (if applicable).

The associative nature of adenylyl transfer catalyzed by T4 DNA ligase

Alexey V. Cherepanov*†‡, Elena V. Doroshenko*†, Jörg Matysik*, Simon de Vries†, and Huub J. M. de Groot*

*Biophysical Organic Chemistry/Solid-State NMR, Leiden Institute of Chemistry, Faculty of Mathematics and Natural Sciences, Leiden University, Einsteinweg 55, 2333CC Leiden, The Netherlands; and †Department of Biotechnology, Faculty of Applied Sciences, Delft University of Technology, Julianalaan 67, 2628 BC Delft, The Netherlands

DNA ligase seals nicks in dsDNA using chemical energy of the phosphoanhydride bond in ATP or NAD^+ and assistance of a divalent metal cofactor Mg^{2+}. Molecular details of ligase catalysis are essential for understanding the mechanism of metal-promoted phosphoryl transfer reactions in the living cell responsible for a wide range of processes, e.g., DNA replication and transcription, signaling and differentiation, energy coupling and metabolism. Here we report a single-turnover ^{31}P solid-state NMR study of adenylyl transfer catalyzed by DNA ligase from bacteriophage T4. Formation of a high-energy covalent ligase–nucleotide complex is triggered *in situ* by the photo release of caged Mg^{2+}, and sequentially formed intermediates are monitored by NMR. Analyses of reaction kinetics and chemical-shift changes indicate that the pentacoordinated phosphorane intermediate builds up to 35% of the total reacting species after 4–5 h of reaction. This is direct experimental evidence of the associative nature of adenylyl transfer catalyzed by DNA ligase. NMR spectroscopy in rotating solids is introduced as an analytical tool for recording molecular movies of reaction processes. Presented work pioneers a promising direction in structural studies of biochemical transformations.

chemical movie | nucleotidyl transfer | structural reaction kinetics | time-resolved cryo–magic-angle-spinning NMR | transition state

U nderstanding chemical mechanics of biocatalysis is a fundamental goal of life sciences. With the development of high-resolution x-ray diffraction analysis and solution NMR a large number of protein structures in the resting state have been solved, giving knowledge on how proteins look, e.g., the detailed view of protein architecture on the primary, secondary, tertiary, and quaternary structure levels. Further insight is coming with studies on how proteins work, e.g., by observing changes of the protein structure in the course of a chemical reaction—recording a molecular movie. Femtosecond laser pulses, molecular beams and ultrafast electron diffraction are used in (in)organic chemistry for monitoring breaking and forming of chemical bonds in real time (1). In biochemistry, kinetic crystallography is used to record molecular movies, an approach that combines starting and stopping the reaction in a protein crystal with x-ray data acquisition at low temperatures (2–8). The successful outcome of a time-resolved x-ray experiment depends as much on a prompt triggering of the reaction as on preparing well diffracting protein crystals. Here we introduce time-resolved low-temperature magic-angle-spinning (cryo-MAS) NMR spectroscopy as a complementary "noninvasive" technique to study catalytic dynamics of biochemical reactions. It combines photo-triggering and freeze-trapping with real-time monitoring of chemical transformations and requires neither protein crystallization nor high intensity penetrating radiation beams. We have assayed the nucleotidyl transfer reaction catalyzed by DNA ligase from bacteriophage T4, a Mg^{2+}- and ATP-dependent enzyme that seals nicks in dsDNA (9). In the first step of catalysis, which was studied in this work, DNA ligase binds ATP, forming a high-energy covalent enzyme–nucleotide complex. Nucleophilic attack on the α-phosphorus of ATP results in

cleavage of the triphosphate moiety, formation of the enzyme-AMP ε-amino lysyl phosphoramidate, and release of the pyrophosphate (10). This reaction is reversible; we have shown that the dimagnesium $ATP \cdot Mg_2$ form is the true substrate for the transfer of adenylyl moiety to the ligase (11). In the reverse reaction, DNA ligase uses the mono-magnesium form of pyrophosphate to synthesize ATP. In the absence of Mg^{2+}, the enzyme binds ATP noncovalently; when Mg^{2+} is added, nucleotidyl transfer starts under pseudo-first-order conditions (11). In the stopped-flow instrument, this reaction is observed as a monophasic process with an activation energy of 16.2 kcal/mol (12). For T4 DNA ligase, ATP and pyrophosphate dissociation constants are <2 and 30 μM, respectively (11). Thus, at the millimolar enzyme concentration used in this work, chemical equilibrium is shifted toward the protein–ligand complexes. After starting the reaction, a dynamic redistribution between the enzyme-bound reactants (RS), reaction intermediates (RI), and product states (PS) is expected. The reaction follows the pathway between the two limiting cases of nucleophilic substitutions shown in Scheme 1. For the fully associative reaction, a penta-coordinated phosphorane intermediate is formed with fractional P–O bond numbers equal to one. The fully dissociative mechanism involves formation of a trigonal metaphosphate intermediate with axial bond numbers close to zero. T4 DNA ligase seals nicks with inversion of configuration at the phosphorus core atom (13), indicating inline substitutions that do not follow the fully dissociative mechanism. The degree to which nucleotidyl transfer is associative is difficult to determine. It is not feasible to characterize transition state (TS) geometry experimentally because of high activation barriers, the associated short lifetimes, and low concentrations. To surpass these experimental limitations, *ab initio* density functional theory (DFT) quantum mechanical (QM)/molecular mechanical (MM) methods are used as an approach for modeling the free-energy landscapes of chemical reactions and characterizing the corresponding TSs *in silico* (14). Substitutions at pentavalent phosphorus have been extensively studied, including enzyme catalysis and assistance of metal cations (15–25). For the associative reactions, calculations in the gas phase show triple-well energy landscapes, with the phosphorane intermediate located in a saddle point between two TSs (22). In the case of the water exchange reaction at the phosphate monoanion (17) or RNA isomerization from a 5′,3′ diester to a 2′,3′ cyclic phosphate diester in hammerhead-ribozyme (20), the assistance of two Mg^{2+} ions favors the associative mechanism and decreases the activation barriers of the reaction. In the first case, the phosphorane intermediate is stabilized by a ≈ 12 kcal/mol potential well and its energy is only
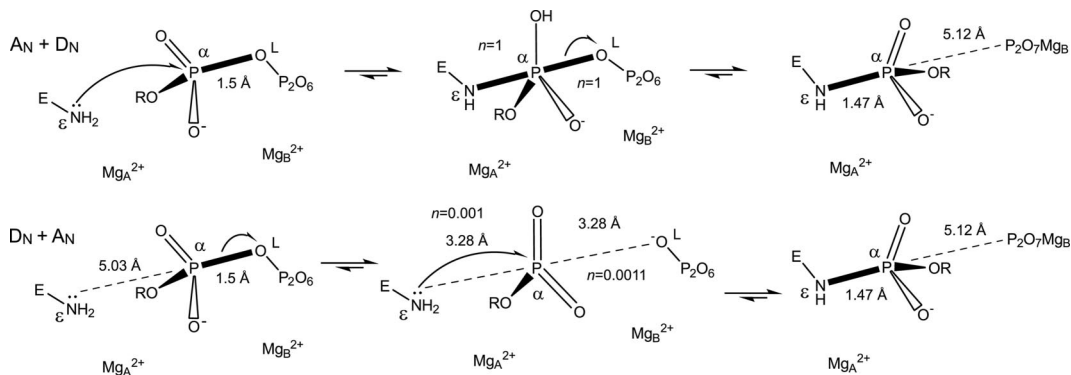
BIOCHEMISTRY

Scheme 1. Two limiting pathways of nucleotidyl transfer catalyzed by DNA ligase. (*Upper*) $A_N + D_N$ (44) is the fully associative mechanism of the inline nucleophilic substitution. The reaction proceeds with the inversion of the stereochemical configuration at the core phosphorus αP. (*Lower*) $D_N + A_N$ is the fully dissociative mechanism. The reaction proceeds with racemization of the product, unless the trigonal metaphosphate intermediate remains tightly bound to the protein, precluding its rotation on the reaction time scale. The distances are taken from the DNA ligase structures 1FVI and 1A0I (45, 46). The 5.12-Å distance between αP and pyrophosphate is taken as an average value of three shortest αP–O distances to the bound sulfate in 1FVI, which is believed to occupy the position of the leaving pyrophosphate (46). The axial bond distances for a trigonal metaphosphate intermediate are taken as half the distance between εN and O_L, averaged between 1FVI and 1A0I. The fractional bond number n for the axial bonds was calculated by using the following equation (47): $D_n = D_r - 0.6 \log(n)$, where D_r is the reference distance for a single covalent bond and D_n is the distance of the bond of interest.

2.69 kcal/mol higher compared with RS (17). In the second case, the energy of the phosphorane intermediate is 8.38 kcal/mol lower than that of RS (20). The intermediate has a reverse activation energy of 8.7 kcal/mol and fractional bond numbers of 0.51 for the nucleophile and 0.67 for the leaving group, calculated by using the bond lengths in RS/RI/PS from ref. 20 and the equation shown in Scheme 1. In principle, this intermediate should accumulate in the reaction mixture in amounts sufficient for experimental detection and characterization under carefully selected pre-steady-state conditions.

In the present work, using time-resolved cryo-MAS NMR methods, we have detected a reaction intermediate in the adenylyl transfer reaction of T4 DNA ligase. Based on the analyses of reaction kinetics and ^{31}P chemical shift values, this intermediate was attributed to a pentacoordinated phosphorane protein–ligand complex. The results presented here give an experimental indication of the associative nature of nucleotidyl transfer performed by DNA ligase on the road to nick repair. Time-resolved solid-state NMR spectroscopy is introduced as an analytic tool for molecular studies of biocatalytic processes, capable of detecting changes in chemical structures of reacting species and correlating these changes to the kinetic and thermodynamic parameters of enzymatic reactions.

Results and Discussion

Time-resolved solid-state NMR studies were performed at cryogenic temperatures with MAS. The experiment included (*i*) preparing a liquid sample of the DNA ligase·ATP complex in the presence of the photolabile caged Mg^{2+}, (*ii*) freeze-quenching the sample in the NMR spectrometer at 240 K, (*iii*) releasing Mg^{2+} from the cage compound by illumination, and (*iv*) monitoring Mg^{2+}-assisted nucleotidyl transfer in real time. DM-nitrophen [1-(2-nitro-4,5-dimethoxyphenyl)-1,2-diaminoethane-*N,N,N′,N′*-tetraacetic acid], an EDTA derivative bearing the 2-nitrophenylethyl moiety on the carbon skeleton (26–28), was used for chelating Mg^{2+}. Illumination of DM-nitrophen triggers the intramolecular redox reaction, in which the 2-nitro group oxidizes a benzylic carbon, leading to a scission of the amino bond with the concomitant increase of K_d^{Mg2+} from 2.5 μM to 3 mM (26). The rate of Mg^{2+} release in our light setup was estimated by using ^{31}P cryo-MAS NMR and caged ATP, a 2-nitrophenylethyl ester at the γ-phosphate (26, 29–31). At 240 K, the apparent photoreaction rate of caged ATP is 1.2 ± 0.2 h^{-1}, which is faster than the observed pseudo-first-order DNA

ligase reaction events. At 21°C and pH 6.9, the rate of Mg^{2+} release from the DM-nitrophen cage is 150-fold faster than the photoreaction rate of caged ATP (32). Thus, we can conclude that the photocleavage of DM-nitrophen does not limit the rate of nucleotidyl transfer catalyzed by T4 DNA ligase. The first reaction event observed in our experiment, binding of Mg^{2+} to the DNA ligase·ATP complex, is limited by self-diffusion of Mg^{2+} to the active site.

At low ionic strength and physiological pH, DNA ligases rapidly precipitate above 10–15 mg/ml protein, which is a ≈10-fold lower concentration than required for the solid-state NMR experiments. To stabilize T4 DNA ligase at higher concentrations, we have used heparin from bovine intestinal mucosa, a commercially available preparation of linear polysaccharide fragments of different lengths. The molecular mass of the fragments is distributed between 9 and 16 kDa, as estimated by size-exclusion chromatography. In complex with heparin, T4 DNA ligase remains fully active in the adenylylation reaction and its solubility greatly increases. Pre-steady-state kinetic analyses show that heparin, similar to the nicked DNA substrate, slows down the second-order binding of ATP, while having minor or no influence on the pseudo-first-order nucleotidyl transfer, depending on pH and Mg^{2+} concentration. In the presence of T4 DNA ligase, heparin forms a gel at 2.5–3.5 mM (31–44 mg/ml), precluding further concentration of the sample. Taking a heparin/protein molar ratio of 0.3:1 we could prepare an 8 mM (44.2% wt/vol) T4 DNA ligase-containing heparin gel, enabling MAS NMR.

^{31}P MAS NMR data of the T4 DNA ligase·ATP complex before the photo release of Mg^{2+} are shown in Fig. 1 (**1**). Peaks at -7.45, -12.28, and -22.84 ppm correspond to the γ-, α-, and β-phosphorus atoms of ligase-bound ATP. In Fig. 1 (**2**), the spectrum of the reaction mixture is shown after the photo release of Mg^{2+} and reacting for 31.5 h at 240 K. The intensities of ATP phosphorus resonances decrease, and two peaks appear at ≈1 ppm. The peak at 0.76 ppm in Fig. 1 (**2**) corresponds to the pyrophosphate product, which can be concluded from the position of the pyrophosphate resonance recorded with the same experimental conditions [Fig. 1 (**3**)]. The peak at 1.9 ppm corresponds to the T4 DNA ligase–AMP product, which can be concluded from the position of the phosphorus resonance of the purified ligase–AMP complex [Fig. 1 (**4**)]. Fig. 1 (**1**) shows that a small amount of the product is formed in the starting mixture of enzyme, ATP, caged Mg^{2+}, and heparin before illumination
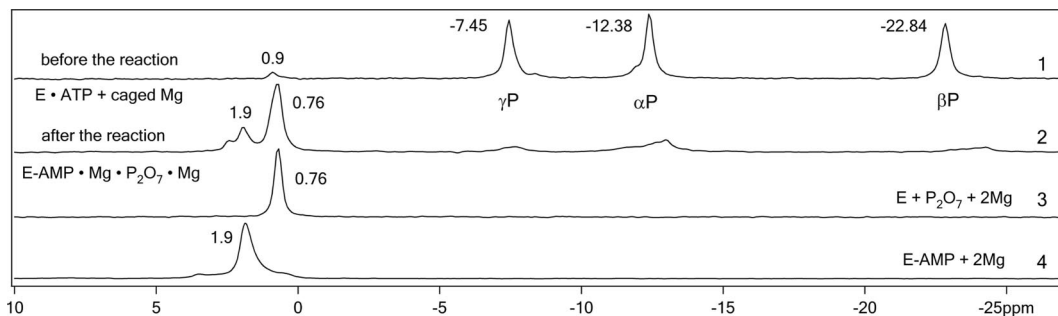
Fig. 1. Proton-decoupled ^{31}P MAS NMR spectra of the T4 DNA ligase·ATP complex, pyrophosphate, and AMP: (**1**) 8 mM T4 DNA ligase, 8 mM ATP, 22 mM DM-nitrophen, 16 mM MgCl$_2$, 2.67 mM heparin in buffer A; (**2**) 8 mM T4 DNA ligase, 8 mM ATP, 22 mM DM-nitrophen, 16 mM MgCl$_2$, 2.67 mM heparin in buffer A after 2-h illumination and 31.5-h reacting at 240 K; (**3**) 8 mM T4 DNA ligase, 8 mM pyrophosphate, 16 mM MgCl$_2$, 2.67 mM heparin in buffer A; (**4**) 8 mM T4 DNA ligase–AMP complex, 16 mM MgCl$_2$, 2.67 mM heparin in buffer A.

(peak at 0.9 ppm). Formation of the product during sample preparation occurs because of dissociation of Mg^{2+} from the chelator complex [$K_d^{Mg2+} \approx 2.5$ μM (26)], binding to the T4 DNA ligase·ATP complex [K_d^{Mg2+}(ATP) ≈ 8.96 μM (33)] and subsequent reaction.

The nucleotidyl transfer reaction catalyzed by T4 DNA ligase was monitored with the ^{31}P signal amplitude-time spectral density plot (SDP) in Fig. 2 *Right*. The intermediates are shown in the reaction scheme in Fig. 2 *Left*. In Fig. 3, the kinetic traces are presented, which are calculated by deconvolution of the SDP and integration of the signals. The isotropic chemical shifts of the intermediates are summarized in Table 1 and are shown in Fig. 2 next to the lines connecting the intermediates to the resonances in the SDP. The intensities, linewidths, and the positions of
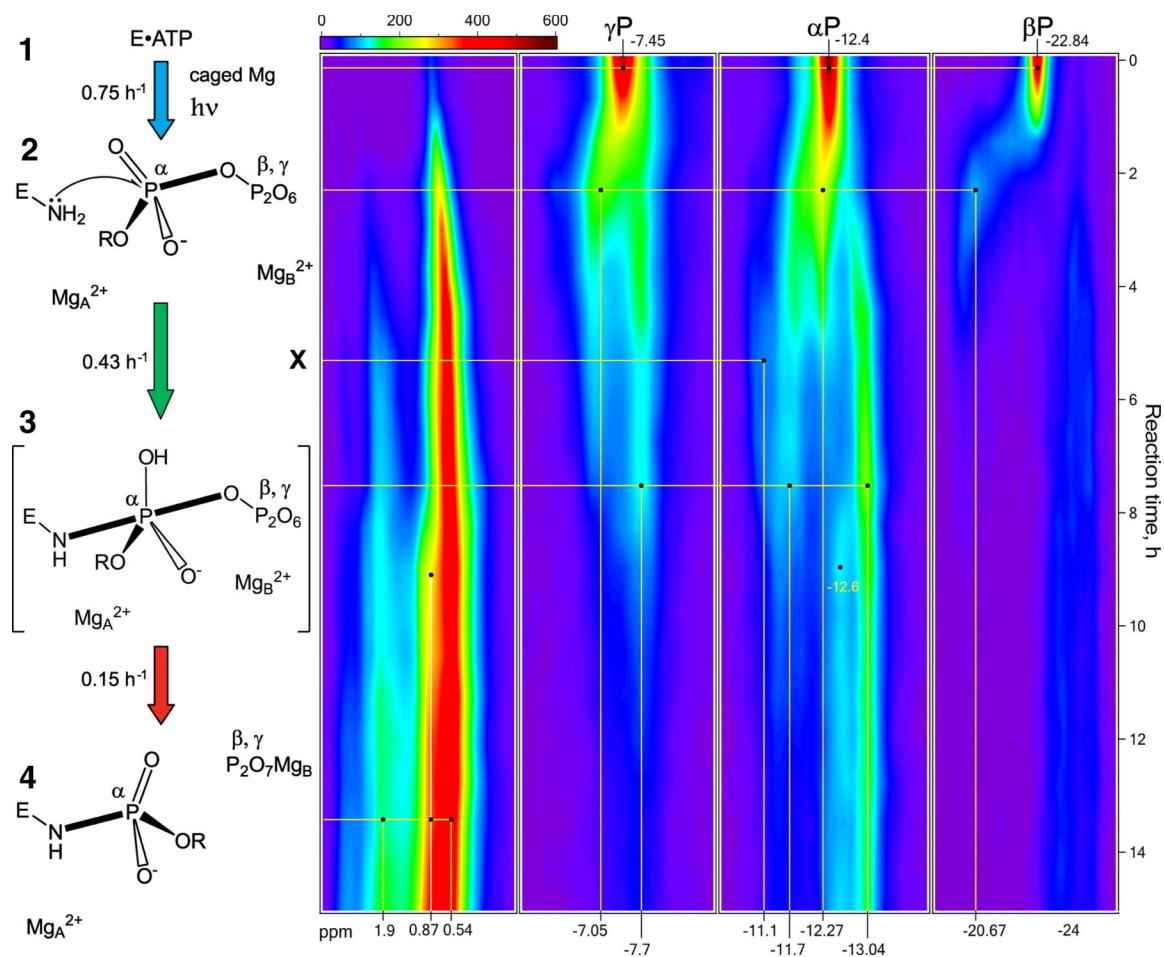

Fig. 2. ^{31}P signal amplitude-time spectral density plot (SDP) of the first 14 h of reaction (*Right*) and the minimal kinetic scheme of the Mg^{2+}-dependent nucleotidyl transfer catalyzed by T4 DNA ligase (*Left*). (**1**) Noncovalent complex E·ATP. (**2**) Quaternary complex E·ATP·Mg$_2$. **X** indicates the putative E·ATP·Mg$_2$ reaction intermediate, in which Mg$_A^{2+}$, in addition to ATP is bound to the protein ligand(s). (**3**) The covalent ternary complex E-NH-ATP·Mg$_2$. (**4**) The adenylylated enzyme in complex with pyrophosphate: E-AMP·Mg·P$_2$O$_7$·Mg; R is the ribosyl adenosine. The color scale shows the amplitude of the proton-decoupled ^{31}P signal. Reaction intermediates on the left are correlated with their resonances in the SDP. The isotropic chemical shifts are indicated.
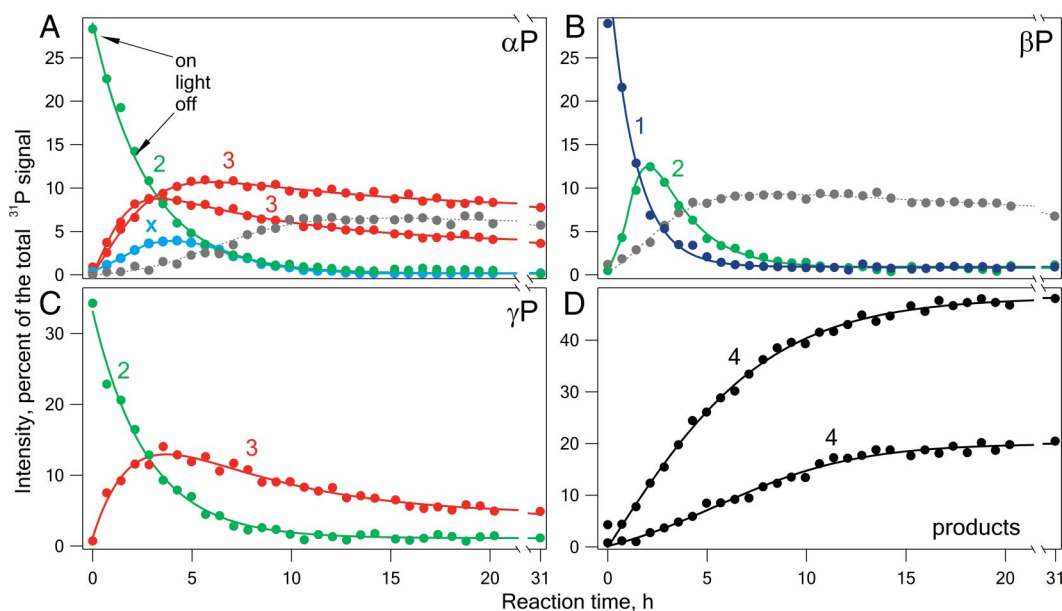
Fig. 3. Kinetics of nucleotidyl transfer catalyzed by T4 DNA ligase. The SDP in Fig. 2 is integrated to determine the total intensity of the ^{31}P signal. The frequency spectrum at each time point is deconvoluted to identify the individual spectral components. The peak areas are expressed as a percentage of the total signal intensity. The standard deviation is 0.1 ppm and 0.5–1% value; error bars are omitted from the graph for clarity. (*A*) Green trace indicates the relative intensity of the αP line of intermediate 2 (αP$_2$) at -12.4 ppm; red is βP$_3$ and αP$_3$ at -13.04 and -11.7 ppm, respectively; light blue is αP$_X$ at -11.1 ppm; gray trace is peak intensity at -12.6 ppm. (*B*) Blue indicates βP$_1$ at -22.84 ppm; green is βP$_2$ at -20.67 ppm; gray is peak intensity between -23 and -24.9 ppm. (*C*) Green trace indicates γP$_2$ between -7.05 and -7.45 ppm; red is γP$_3$ at -7.7 ppm. (*D*) (*Upper*) Sum of relative intensities of the pyrophosphate resonances (βP$_4$ and γP$_4$) between 1.2 and 0 ppm. (*Lower*) The relative intensity of the phosphorus signal of the enzyme-adenylylate (αP$_4$) between 3 and 1.2 ppm.

almost all ^{31}P resonances gradually change during the reaction. At 240 K, the fastest observable process (0.75 ± 0.3 h^{-1}) is a downfield shift of the ATP resonances, which reflects binding of Mg^{2+} to the noncovalent DNA ligase·ATP complex 1, forming E·ATP·Mg$_2$, the catalytically competent quaternary complex 2. In the reaction scheme in Fig. 2, the binding of Mg^{2+} is indicated by the blue arrow. The βP resonance of 1 (βP$_1$) at -22.84 ppm experiences the most pronounced downfield shift of ≈ 2.7 ppm, matching the shift of βP for ATP in solution (34). The βP$_1$ line is well separated from βP$_2$; its kinetic trace is shown in Fig. 3 (1), in blue. During binding of Mg^{2+}, the γP$_1$ line shifts by ≈ 0.4 ppm; the shift of the αP$_1$ line is the smallest, ≈ 0.13 ppm. The kinetic traces for γP$_1$ and αP$_1$ resonances could not be resolved because of their strong spectral overlap with γP$_2$ and αP$_2$.

Fig. 2 shows that the spectra of the intermediate states observed during binding of Mg^{2+} cannot be obtained by superposition of the resonances of 1 and 2. Mg^{2+} causes a synchronized gradual change of chemical environment around the ^{31}P nuclei when it is approaching. Hence the lines of 1 gradually and continuously shift, becoming the lines of 2 once Mg^{2+} reaches its position in the active site. Similar shifts can be seen on a longer time scale in the αP region, around -11.1 ppm, in the γP region (shift from -7.45 to -7.05 ppm), and at ≈ 0 ppm. In the course of the reaction, the pyrophosphate resonances are becoming

nonidentical (0.54 and 0.87 ppm), either because of the conformational change of the enzyme, protonation events, or chemistry-driven spatial charge rearrangement.

Formation of the catalytically competent complex 2 triggers the nucleotidyl transfer reaction, which is indicated by the green arrow in the reaction scheme in Fig. 2. The E·ATP·Mg$_2$ resonances at -7.05, -12.27, and -20.67 ppm decay with $k_{obs} = 0.43 \pm 0.3$ h^{-1} (Fig. 3, 2, green) and a reaction intermediate 3 emerges at -7.7, -11.7, and -13.04 ppm; its βP resonance is shifted ≈ 7 ppm further downfield compared with βP$_2$ (Fig. 2 and Table 1). After 4–5 h of reaction, 3 accumulates to 35% of the total ^{31}P signal (Fig. 3, 3, red), assuming that the relaxation times for the observed species are similar. 3 is converted to the product state 4, enzyme–adenylylate complex with pyrophosphate, with $k_{obs} = 0.15 \pm 0.03$ h^{-1} (Fig. 3, 4, black). In the reaction scheme in Fig. 2, conversion 3 → 4 is indicated by the red arrow. Preliminary radio frequency dipolar recoupling experiments at 240 K reveal chemical-shift correlations βP$_3$–αP$_4$ and γP$_3$–βP$_4$, indicating that 3 is interconverting with 4 within the 7-ms mixing time via an elementary bond breaking/forming step. Judging the reaction kinetics, the intermediate 3 can be assigned to a pentacoordinated phosphorane E-NH-ATP·Mg$_2$, indicating that nucleotidyl transfer catalyzed by T4 DNA ligase follows the associative pathway. This conclusion is supported by the observation that 3 has the resonances of the triphosphate moiety. In addition, the βP$_3$ resonance is shifted ≈ 10 ppm downfield compared with βP$_1$, which indicates a decrease of electronic polarization at the βP after formation of the phosphoramidate bond. In the reaction scheme in Fig. 2, 3 is shown with Mg^{2+} ions poised for catalysis according to the two-metal-ion mechanism of nucleotidyl transfer catalyzed by DNA- and RNA-dependent DNA and RNA polymerases (35, 36). Two-metal-ion assisted incorporation of dCTP in the nascent primer chain catalyzed by DNA polymerase β has been recently examined by using an empirical valence bond QM/MM modeling approach at 310 K (24). The pentacoordinated phosphorane intermediate was

Table 1. Isotropic chemical shifts for the ^{31}P signals of the observed reacting species

RI	$\delta_{\alpha P}$	$\delta_{\beta P}$	$\delta_{\gamma P}$
1	-12.38	-22.84	-7.45
2	-12.27	-20.67	-7.05
X	-11.1	ND	ND
3	-11.7	-13.04	-7.7
4	1.9	0.87, 0.54	

ND, not detected.

Cherepanov *et al.*

shown to have an 11.4 kcal/mol higher energy compared with RS and the activation barriers of 13.9 and 15.7 kcal/mol, which correspond to the PO bond-forming and bond-breaking steps, respectively. The phosphorane moiety was calculated to carry a negative charge of ≈ 2.3 electronic equivalents (compare table 1 in ref. 24), which may account for the high energy of an intermediate and a shallow potential well. The analogous phosphorane intermediate was characterized for T7 DNA polymerase (36). In the latter case, its energy is only 4.8 kcal/mol higher than that of RS. The activation barriers for PO bond forming and breaking steps are 13.7 and 13.8 kcal/mol, respectively. The predicted phosphorane lifetime is 10^{-6} s at 298 K. In our experiments, in a solid heparin-protein glass, favorable thermodynamic changes, e.g., loss of activation entropy may slow down the reaction and extend the lifetime from micro/milliseconds at 298 K to hours at 240 K. Non-Arrhenius slowing of chemical processes is a common phenomenon in cryobiochemistry (37). After activation by light, a photoactive protein goes through a sequence of intermediates that can be trapped by freezing. This has been demonstrated in solid-state NMR studies of the photocycle of bacteriorhodopsin and the photosequence of rhodopsin (38, 39).

The kinetic analyses suggest that an additional intermediate **X** follows **2**, preceding the phosphorane **3**: a minor resonance around -11.1 ppm appears with $k_{obs} = 0.55 \pm 0.06$ h^{-1} and decays with $k_{obs} = 0.41 \pm 0.03$ h^{-1} (Fig. 3, X, light blue). Using pre-steady-state kinetic analyses, we have shown that the K_d for Mg$_A^{2+}$ decreases from 16.7 to 1.4 mM after ATP·Mg$_2$ binds to T4 DNA ligase, forming **2** (11). To account for that, we have suggested that Mg$_A^{2+}$ forms an extra coordination bond to the catalytic Lys-159 in the quaternary complex, promoting making and breaking of chemical bonds by bringing together the participating nucleophiles and compensating negative charges. Mg$_A^{2+}$ can bind to other residues in the active site, e.g., Asp-29, which is 3.31 or 5.16 Å (O—O) away from the α-phosphate in ligase–adenylylate (40) or the ligase–adenylylate complex with nicked dsDNA (41), respectively, taking the known structure of DNA ligase from *Chlorella* virus PBCV-1. Thus, **2** could be an encounter quaternary complex, in which Mg$_A^{2+}$ coordinates to the ATP phosphate oxygen atoms and water, whereas **X** could be the enzyme-stabilized complex, where Mg$_A^{2+}$ is additionally bound to the protein ligand(s) in the last stance before formation of the phosphoramidate bond in **3**. Binding of protein ligands to Mg$_A^{2+}$ would involve a minor coordination change at the α-phosphate, and the chemical shifts of the β- and γ-phosphorus nuclei of **X** are expected to be identical to **2**.

Some extra species are present during the reaction: e.g., a resonance at -12.6 ppm ($k_{obs} = 0.18 \pm 0.02$ h^{-1}; Fig. 3A, gray), and two resonances at -23.46 and -24.34 ppm (Fig. 3B, gray, united trace), which appear with $k_{obs} = 0.43 \pm 0.04$ h^{-1} and equilibrate with $k_{obs} = 0.01 \pm 0.005$ h^{-1}. The latter two bear mechanistic importance; in the experiments with caged ATP and

DNA ligase from *Chlorella* virus PBCV-1 similar resonances are observed. These signals can be attributed to the dinucleoside tetraphosphate Ap$_4$A, which is formed when ATP is present in excess to the enzyme (42). As estimated from kinetic analyses of the SDP in Fig. 2, the ATP excess in the reaction mixture is <7%, within experimental error of the protein concentration value.

The results presented here demonstrate the power and potential of cryo-MAS NMR spectroscopy in studies of molecular dynamics associated with biocatalysis. In the case of nucleotidyl transfer catalyzed by T4 DNA ligase we have characterized the transient reaction species in a set of time-resolved ^{31}P experiments, i.e., recorded a chemical movie of bond breaking and forming without solving the molecular structure of the entire protein–ligand complex. NMR spectroscopy in rotating solids has been used for detecting changes of the environment around the observed nuclei as the chemical process advances over the energy barrier along the reaction coordinate. In principle, with multidimensional cryo-MAS NMR experiments it should be possible to assign this motion to well defined conformational changes in a space-time continuum and record a 3D molecular movie of a biochemical reaction. In combination with molecular modeling of the high-energy transition states and extended to other protein–ligand complexes, this approach might bring a detailed understanding of the modus operandi of the uniquely evolved biological catalysts, the enzymes.

Materials and Methods

Recombinant T4 DNA ligase was diluted to 3 mg/ml in 70 mM Tris·HCl (pH 7.5), 50 mM KCl, and 2 mM Tris(2-carboxyethyl)phosphine (TCEP) (buffer A) at 4°C. Heparin from bovine intestinal mucosa (Fluka; 51536) was added to the protein solution at 0.3:1 heparin/ligase molar ratio, taking M_w for heparin of 12.5 kDa. The protein–heparin mixture was concentrated to 5 mM protein (170 μl, 280 mg/ml ligase) on a 10-kDa cutoff filter (Centriprep/Centricon concentrators; Amicon). ATP was added to a final concentration of 8 mM, followed by DM-nitrophen/MgCl$_2$ solution (1.5:1 molar ratio), which was added in the dark to a final concentration of 16 mM Mg^{2+}. The sample was concentrated to 100 μl (10-kDa cutoff Microcon concentrator; Amicon; 1.5 h), yielding 442 mg/ml (8 mM) ligase, transferred to the 4 mm ZrO$_2$ MAS rotor ($\approx$40 mg of protein), stored on ice, and loaded in the spectrometer within 2 h after preparation. A 17.5-T wide bore Bruker Avance NMR spectrometer with MAS probe modified for the light-driven experiments (43) was used for data acquisition. Proton-decoupled ^{31}P MAS NMR spectra with a recycle delay d1 = 0.1 s were recorded at 240 K and 7-kHz spinning rate; the chemical shifts of phosphorus resonances were recorded relative to (NH$_4$)$_3$PO$_4$. Each spectrum contained 20,480 scans (spectrum acquisition time expt = 42:36 min). Light (380–780 nm) from a 1-kW Xenon arc light source was turned on for 2 h after acquisition of the first spectrum. Igor Pro software (Wavemetrics) was used for data analysis. The deconvolution of SDP shown in Fig. 2 was performed by using the Igor Pro multipeak fitting package.

1. Zewail AH (2003) Femtochemistry: Atomic scale dynamics of the chemical bond using ultrafast lasers. *Nobel Lectures, Chemistry 1996–2000*, ed Grenthe I (World Scientific, Singapore), pp 274–367.
2. Bourgeois D, Royant A (2005) Advances in kinetic protein crystallography. *Curr Opin Struct Biol* 15:538–547.
3. Bourgeois D, Schotte F, Brunori M, Vallone B (2007) Time-resolved methods in biophysics. 6. Time-resolved Laue crystallography as a tool to investigate photo-activated protein dynamics. *Photochem Photobiol Sci* 6:1047–1056.
4. Helliwell R (1986) Reflections on a decade of synchrotron X-radiation protein crystallography. *Rigaku J* 3:3–12.
5. Kack H, Gibson KJ, Lindqvist Y, Schneider G (1998) Snapshot of a phosphorylated substrate intermediate by kinetic crystallography. *Proc Natl Acad Sci USA* 95:5495–5500.
6. Katona G, et al. (2007) Raman-assisted crystallography reveals end-on peroxide intermediates in a nonheme iron enzyme. *Science* 316:449–453.
7. Neutze R, Huldt G, Hajdu J, van der Spoel D (2004) Potential impact of an x-ray free electron laser on structural biology. *Radiat Phys Chem* 71:905–916.
8. Ren Z, et al. (1999) Laue crystallography: Coming of age. *J Synchrotron Rad* 6:891–917.
9. Lehman IR (1974) DNA ligase: Structure, mechanism, and function. *Science* 186:790–797.
10. Gumport RI, Lehman IR (1971) Structure of the DNA ligase-adenylate intermediate: Lysine (ε-amino)-linked adenosine monophosphoramidate. *Proc Natl Acad Sci USA* 68:2559–2563.
11. Cherepanov AV, de Vries S (2002) Kinetic mechanism of the Mg^{2+}-dependent nucleotidyl transfer catalyzed by T4 DNA and RNA ligases. *J Biol Chem* 277:1695–1704.
12. Cherepanov AV, de Vries S (2003) Kinetics and thermodynamics of nick sealing by T4 DNA ligase. *Eur J Biochem* 270:4315–4325.
13. Mizuuchi K, Nobbs TJ, Halford SE, Adzuma K, Qin J (1999) A new method for determining the stereochemistry of DNA cleavage reactions: Application to the SfiI and HpaII restriction endonucleases and to the MuA transposase. *Biochemistry* 38:4640–4648.
14. Ridder L, Mulholland AJ (2003) Modeling biotransformation reactions by combined quantum mechanical/molecular mechanical approaches: From structure to activity. *Curr Top Med Chem* 3:1241–1256.
15. Berente I, Beke T, Náray-Szabó G (2007) Quantum mechanical studies on the existence of a trigonal bipyramidal phosphorane intermediate in enzymatic phosphate ester hydrolysis. *Theor Chim Acta* 118:129–134.

BIOCHEMISTRY

16. De Vivo M, Cavalli A, Carloni P, Recanatini M (2007) Computational study of the phosphoryl transfer catalyzed by a cyclin-dependent kinase. *Chem Eur J* 13:8437–8444.
17. Kamerlin SC, Wilkie J (2007) The role of metal ions in phosphate ester hydrolysis. *Org Biomol Chem* 5:2098–2108.
18. Kapustina M, Carter CW, Jr (2006) Computational studies of tryptophanyl-tRNA synthetase: Activation of ATP by induced-fit. *J Mol Biol* 362:1159–1180.
19. Klahn M, Rosta E, Warshel A (2006) On the mechanism of hydrolysis of phosphate monoesters dianions in solutions and proteins. *J Am Chem Soc I* 128:15310–15323.
20. Leclerc F, Karplus M (2006) Two-metal-ion mechanism for hammerhead-ribozyme catalysis. *J Phys Chem B* 110:3395–3409.
21. Lopez X, Dejaegere A, Leclerc F, York DM, Karplus M (2006) Nucleophilic attack on phosphate diesters: A density functional study of in-line reactivity in dianionic, monoanionic, and neutral systems. *J Phys Chem B* 110:11525–11539.
22. van Bochove MA, Swart M, Bickelhaupt MF (2007) Nucleophilic substitution at phosphorus centers (S_N2). *ChemPhysChem* 8:2452–2463.
23. Wang L, Yu X, Hu P, Broyde S, Zhang Y (2007) A water-mediated and substrate-assisted catalytic mechanism for *Sulfolobus solfataricus* DNA polymerase IV. *J Am Chem Soc I* 129:4731–4737.
24. Xiang Y, Goodman MF, Beard WA, Wilson SH, Warshel A (2008) Exploring the role of large conformational changes in the fidelity of DNA polymerase β. *Proteins* 70:231–247.
25. Xiang Y, Warshel A (2008) Quantifying free energy profiles of proton transfer reactions in solution and proteins by using a diabatic FDFT mapping. *J Phys Chem B* 112:1007–1015.
26. Kaplan JH, Ellis-Davies GC (1988) Photolabile chelators for the rapid photorelease of divalent cations. *Proc Natl Acad Sci USA* 85:6571–6575.
27. Grell E, *et al.* (1989) Caged-Ca^{2+}: A new agent allowing liberation of free Ca^{2+} in biological systems by photolysis. *Cell Mol Biol* 35:515–522.
28. McCray JA, Fidler-Lim N, Ellis-Davies GC, Kaplan JH (1992) Rate of release of Ca^{2+} following laser photolysis of the DM-nitrophen-Ca^{2+} complex. *Biochemistry* 31:8856–8861.
29. Kaplan JH, Forbush B, 3rd, Hoffman JF (1978) Rapid photolytic release of adenosine 5′-triphosphate from a protected analogue: Utilization by the Na:K pump of human red blood cell ghosts. *Biochemistry* 17:1929–1935.
30. McCray JA, Herbette L, Kihara T, Trentham DR (1980) A new approach to time-resolved studies of ATP-requiring biological systems: Laser flash photolysis of caged ATP. *Proc Natl Acad Sci USA* 77:7237–7241.
31. Walker JW, Reid GP, McCray JA, Trentham DR (1988) Photolabile 1-(2-nitrophenyl)ethyl phosphate esters of adenine nucleotide analogs: Synthesis and mechanism of photolysis. *J Am Chem Soc* 110:7170–7177.
32. Barth A, Hauser K, Maentele W, Corrie JET, Trentham DR (1995) Photochemical release of ATP from ''caged ATP'' studied by time-resolved infrared spectroscopy. *J Am Chem Soc* 117:10311–10316.
33. Frey CM, Banyasz JL, Stuehr JE (1972) Interactions of divalent metal ions with inorganic and nucleoside phosphates. II. Kinetics of magnesium(II) with $HP_3O_{10}^{4-}$, ATP, CTP, $HP_2O_7^{3-}$, ADP, and CDP. *J Am Chem Soc I* 94:9198–9204.
34. Brown SG, Hawk RM, Komoroski RA (1993) Competition of Li(I) and Mg(II) for ATP binding: A ^{31}P NMR study. *J Inorg Biochem* 49:1–8.
35. Batra VK, *et al.* (2006) Magnesium-induced assembly of a complete DNA polymerase catalytic complex. *Structure (London)* 14:757–766.
36. Florian J, Goodman MF, Warshel A (2005) Computer simulations of protein functions: Searching for the molecular origin of the replication fidelity of DNA polymerases. *Proc Natl Acad Sci USA* 102:6819–6824.
37. Douzou P (1977) *Cryobiochemistry: An Introduction* (Academic, San Francisco).
38. Herzfeld J, Lansing JC (2002) Magnetic resonance studies of the bacteriorhodopsin pump cycle. *Annu Rev Biophys Biomol Struct* 31:73–95.
39. Smith SO, de Groot HJM, Gebhard R, Lugtenburg J (1992) Magic angle spinning NMR studies on the metarhodopsin II intermediate of bovine rhodopsin: Evidence for an unprotonated Schiff base. *Photochem Photobiol* 56:1035–1039.
40. Odell M, Malinina L, Sriskanda V, Teplova M, Shuman S (2003) Analysis of the DNA joining repertoire of *Chlorella* virus DNA ligase and a new crystal structure of the ligase-adenylate intermediate. *Nucleic Acids Res* 31:5090–5100.
41. Nair PA, *et al.* (2007) Structural basis for nick recognition by a minimal pluripotent DNA ligase. *Nat Struct Mol Biol* 14:770–778.
42. Madrid O, *et al.* (1998) T4 DNA ligase synthesizes dinucleoside polyphosphates. *FEBS Lett* 433:283–286.
43. Matysik J, *et al.* (2000) A set-up to study photochemically induced dynamic nuclear polarization in photosynthetic reaction centres by solid-state NMR. *Ind J Biochem Biophys* 37:418–423.
44. Guthrie RD (1989) System for symbolic representation of reaction mechanisms. *Pure Appl Chem* 61:23–56.
45. Subramanya HS, Doherty AJ, Ashford SR, Wigley DB (1996) Crystal structure of an ATP-dependent DNA ligase from bacteriophage T7. *Cell* 85:607–615.
46. Odell M, Sriskanda V, Shuman S, Nikolov DB (2000) Crystal structure of eukaryotic DNA ligase-adenylate illuminates the mechanism of nick sensing and strand joining. *Mol Cell* 6:1183–1193.
47. Pauling L (1960) *The Nature of the Chemical Bond* (Cornell Univ Press, Ithaca, NY).

Cherepanov *et al.*